Pathway-resolved decomposition demonstrates correlation and noise dependencies of redundant information processing in recurrent feed-forward topologies

Ayan Biswas *
Department of Chemistry, Bose Institute, 93/1 A P C Road, Kolkata 700009, India

(Received 6 October 2021; accepted 4 February 2022; published 14 March 2022)

In a biochemical assay that converts fan-in networks into feed-forward loops (FFLs), we show that the inter-regulator redundant information about the output gene product can be decomposed into finer components, mediated by the constituent pathways. Variance-based information within the linear noise regime facilitates quantifying these submodular redundancies. Contrary to the conventional wisdom on information decomposition, we report that information redundancy depends nontrivially on inter-regulator correlation. For the type-1 coherent (C1) and incoherent (I1) FFLs, the direct regulatory path-mediated redundancy is certainly correlation independent. However, components induced by the indirect regulatory path and interpathway interference are correlation dependent in (non)linear fashion. The trade-off between information redundancy and similarly decomposable extrinsic noise from input to output node has been demonstrated for the pathways and full motifs. Our analyses suggest that the interpathway cross redundancy positively and negatively influences the superposition of elementary redundancies in the C1- and I1-FFLs, respectively. Their corresponding total extrinsic noise is produced by the weighted sum and difference of the pathway-specific components. We find that the I1-FFL is able to manufacture more varied redundancy and extrinsic noise responses compared to the C1-FFL. Underlying the differing characteristics of the composite metrics across FFL variants, there exist uniformly behaving pathway-dependent elements. The decomposition framework has been meticulously explored in biologically rational parametric realizations through analytical estimates and stochastic simulations.

DOI: 10.1103/PhysRevE.105.034406

I. INTRODUCTION

A living cell maintains its fitness by coping with environmental dynamics through a continual flow of predictive information. Over the years, many biophysical problems, such as chemotaxis, metabolism, cell signaling, intercellular resource sharing, quorum sensing, inflammatory response, morphogenesis, cellular decision making, and neural coding, have benefited from information-theoretic insights [1–8]. In gene regulation, information from an external signal is processed by the cell's finely constructed networks of biochemical entities. When the input species relays this signal to the output gene, necessary biomolecules are synthesized at the appropriate time and quantity. To this end, specialized regulatory proteins are often required to control the output gene expression. With ∼4500 genes [9] and $O(10^7)$ proteins [10], the *E. coli* gene regulatory network is a model complex system displaying distinct properties at the collective and subsystem levels. The bacterial and yeast transcription networks are dense in statistically over-represented network motifs which play crucial roles in various physiological processes [11,12].

A feed-forward loop (FFL) is a common motif in these systems and consists of three gene products with two upstream regulators controlling the output expression. Unlike in the simple regulation or fan-in network where the regulators are independent, the top-level master regulator of an FFL enslaves the intermediate co-regulator. As a result, an FFL has two signal decoding channels running in parallel. A one-step cascade is formed by connecting the master regulator to the output, but a two-step cascade places the co-regulator between the other two species. In a random net, eight FFLs cover all possible combinations of activatory and inhibitory edges. The C1- and I1-FFLs are preferred by the bacterial and yeast gene transcription networks [13]. All of the edges in the C1-FFL are activatory in nature, whereas an inhibitory edge connects the co-regulator to the output in the I1-FFL. Experiments on *E. coli* reveal that AND-gated C1- and I1-FFLs, respectively, control the *ara* and *gal* metabolic systems, whereas a SUM-gated C1-FFL regulates the flagella-producing *fli* operon [14–16].

Shannon's information theory [17] has lately been extended in the form of the *partial information decomposition* (PID) principle [18,19] to tackle multivariate systems. This is particularly useful in dealing with an interacting biochemical population where the summed pairwise information differs from the ensemble-level information. In this domain, a long-standing problem has been the negative-valued *interaction information*, an unphysical outcome given that the metric signifies the common entropy space of three or more random variables. To resolve this discrepancy, PID quantifies the finer substructures of multivariate information. These non-negative and independent elements are referred to as *unique, synergistic*, and *redundant* information. For the well-characterized

*ayanbiswas19@gmail.com

three-variable Gaussian system with two information sources (drivers) and one target species, the unique information is solely provided by the individual sources, whereas the synergy appears from their complementary interaction. The redundancy exists due to the presence of a common intersource information space. Thanks to PID, the interaction information that weighs the total information against the summed pairwise information is proved identical to the difference between synergy and redundancy. Therefore, a positive (negative) interaction information merely reflects the prevalence of synergy (redundancy) in multispecies interaction. At times, synergy and redundancy may balance each other to produce zero interaction information. A fully specified decomposition rule conceives of redundancy as the minimum of the two constituent pairwise mutual information. As a corollary, information redundancy is regarded to be independent of the intersource correlation strength [19]. This concept is an integral part to any analysis based on the *minimum mutual information* PID (MMI PID) [19] and is the central theme of our present investigation. Prior to the inception of MMI PID, a number of other PID measures were introduced by different information theorists. Some of them formalized redundancy [18,20], while others built on synergy [21,22]. The common assumption is that the redundant information and the unique information only depend on the marginal distributions between each of the sources and the target. For sources with arbitrary dimensions and a univariate target jointly forming a multivariate Gaussian distribution, MMI PID unified the earlier PIDs. Within this framework, the unique information from the source responsible for the minimum mutual information vanishes. Synergy appears as the extra information from the weaker source when the stronger one is known. Both redundancy and synergy maintain symmetry in relation to the sources.

The three-species-strong FFL topology is suitable for a correlation-based description of redundant information processed by the regulators targeting their common output. Therefore, we hypothesize a biochemical construct that starts from fan-in networks and gradually increases the inter-regulator interaction to generate the C1- and I1-FFLs. Our theoretical assay is inspired by previous experiments that compared the relative physiological advantages of these structures in *E. coli* [14]. We quantify the inter-regulator correlation strength in terms of the co-regulator species abundance synthesized by the master regulator. In the spirit of PID, we present a pathway-dependent decomposition of redundant information in the C1- and I1-FFLs. In doing so, nontrivial correlation patterns of information redundancy emerge. This decomposition is realizable if we choose to compute information in terms of a reduction in variance instead of the conventional reduction in entropy. Since stochasticity is ubiquitous in biochemical systems with both beneficial and detrimental effects [23,24], we present an analytically tractable correspondence between information redundancy and noise flow in FFLs. To this end, we use the definition of extrinsic noise as elucidated in the dual-reporter technique of Elowitz *et al.* [25].

To model the FFL dynamics, we apply the Langevin formalism [26,27] where s, x, and y indicate copy numbers of

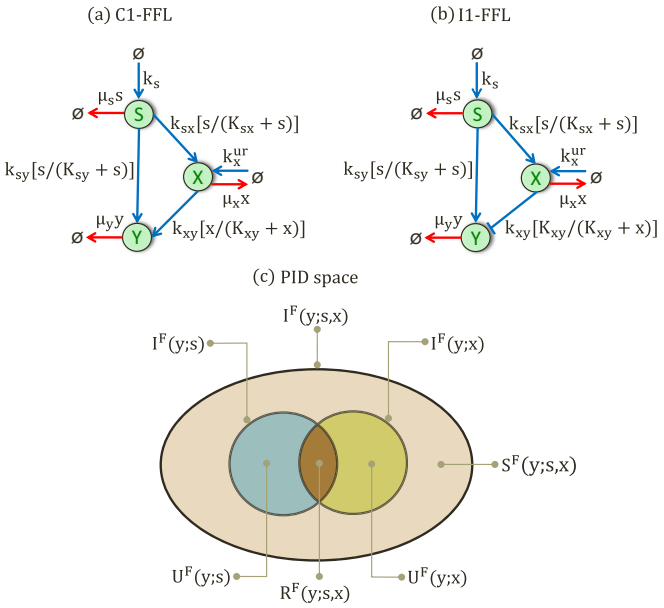

FIG. 1. (a), (b) The schematic diagrams of the C1- and I1-FFLs, respectively, with production (degradation) reactions marked by blue (red) arrows and associated propensities. The Venn diagram in (c) is reproduced from Ref. [19] and shows generic PID elements embedded within the pairwise information [$I^F(y;s)$ and $I^F(y;x)$] and total information [$I^F(y;s,x)$] spaces. Here, $\{s,x\}$ act as information sources, with y as their common target. $U^F(y;s)$ [$U^F(y;x)$] is the unique information from s (x) about y. $R^F(y;s,x)$ and $S^F(y;s,x)$ are the redundant information and synergistic information from $\{s,x\}$ about y, respectively. These PID elements are interconnected through the equations [19]: $I^F(y;s) = U^F(y;s) + R^F(y;s,x)$, $I^F(y;x) = U^F(y;x) + R^F(y;s,x)$, and $I^F(y;s,x) = U^F(y;s) + U^F(y;x) + R^F(y;s,x) + S^F(y;s,x)$.

the master regulator, co-regulator, and output gene product, respectively:

$$\frac{ds}{dt} = f_s - \mu_s s + \sqrt{\beta_s(s)}\xi_s(t), \tag{1a}$$

$$\frac{dx}{dt} = f_x(s) - \mu_x x + \sqrt{\beta_x(s,x)}\xi_x(t), \tag{1b}$$

$$\frac{dy}{dt} = f_y(s,x) - \mu_y y + \sqrt{\beta_y(s,x,y)}\xi_y(t). \tag{1c}$$

Figures 1(a) and 1(b) represent the C1- and I1-FFLs with blue (red) arrows denoting the production (degradation) reactions with propensities $f_i(\mu_i i)$. We have used Hill functions to model the co-regulator and output productions, i.e., $f_x(s) = k_x^{ur} + k_{sx}[s/(K_{sx}+s)]$, $f_y(s,x) = k_{sy}[s/(K_{sy}+s)] + k_{xy}[x/(K_{xy}+x)]$ (C1), and $f_y(s,x) = k_{sy}[s/(K_{sy}+s)] + k_{xy}[K_{xy}/(K_{xy}+x)]$ (I1). Here, $k_{...}$ (μ_i) stands for the production (degradation) rate parameter. In particular, k_x^{ur} is the rate parameter for unregulated synthesis of the co-regulator. This reaction keeps the three-node structures intact when the edge $S \to X$ is absent. Thus, appear the fan-in topologies [9], which act as primers for constructing the C1- and I1-FFLs. K_{sx} is the activation coefficient which is numerically equivalent to the master regulator's population needed to produce the half-maximal regulated co-regulator abundance. In mechanistic terms,

$K_{sx} = \sigma^u_{sx}/\sigma^b_{sx}$, where σ^u_{sx} and σ^b_{sx} are the unbinding and binding rate parameters for the master regulator to bind to its co-regulator, respectively [28]. Other $K_{\cdots}$ follow similar interpretation. K_{xy} works as the repression coefficient in the I1-FFL. $\xi_i(t)$ are statistically independent and temporally uncorrelated Gaussian white noise terms with zero means and unit variances. β_i are the corresponding dynamical noise strengths [27]. Recent advances in the MMI PID literature are based on Gaussian random variables and this motivates us to use the linear noise approximation (LNA). LNA is obtained by applying van Kampen's system size (Ω) expansion to the multivariate master equation corresponding to the former Langevin description in the close proximity of stationary trajectories [26,29]. Within this regime, fluctuation around the monostable deterministic mean population is assumed to be small for large Ω (in the strict mathematical sense, when $\Omega \to \infty$). The approximated random variable is given by $i = \Omega\rho_i + \sqrt{\Omega}\delta i$, where ρ_i and δi are, respectively, the macroscopic concentration and the copy number fluctuation of the ith species. The stationary solution of the resulting linear Fokker-Plank equation is a mutivariate Gaussian whose covariance matrix ($\boldsymbol{\Sigma}$) obeys the Lyapunov equation: $\boldsymbol{J\Sigma} + \boldsymbol{\Sigma J}^T + \boldsymbol{D} = \boldsymbol{0}$. $\boldsymbol{J}$ and $\boldsymbol{D}$ are the steady-state Jacobian and noise (diffusion) matrices, respectively. For our case, we normalize the system volume to unity without any loss of generality. This is motivated by the fact that in a eukaryotic cell, the regulatory proteins are synthesized in the cytoplasm and then transported to the nucleus. Hence, the volume sensed by them is neither cytoplasmic nor nuclear volume, but an effective cellular volume [30]. In this measurement setup, the copy number and concentration states become numerically identical to each other. Previously, this choice was validated for systems free of bimolecular reactions [31,32]. The information-theoretic analyses of four-node regulatory topologies by Ziv *et al.* successfully capitalized on this simplifying assumption in the presence of Hill-type activatory and inhibitory input functions with cooperative effects [33]. When the fluctuations around mean copy numbers are smaller than the respective mean sizes, we can use $\langle f_i(\cdot)\rangle \approx f_i(\langle\cdot\rangle)$ in Eqs. (1a)–(1c). Here, $\langle\cdot\rangle$ refers to the steady-state ensemble average. Thus, we arrive at the following expressions: $\langle s\rangle = k_s/\mu_s$, $\langle x_{ur}\rangle = (k^{ur}_x/\mu_x)$, $\langle x_s\rangle = (k_{sx}/\mu_x)[\langle s\rangle/(K_{sx} + \langle s\rangle)]$. Here, $\langle x_{ur}\rangle$ and $\langle x_s\rangle$, respectively, denote the unregulated and regulated co-regulator populations which additively produce the total population $\langle x\rangle$. Similarly, for the output, the directly and indirectly regulated populations are, respectively, $\langle y_s\rangle = (k_{sy}/\mu_y)[\langle s\rangle/(K_{sy} + \langle s\rangle)]$ and $\langle y_x\rangle = (k_{xy}/\mu_y)[\langle x\rangle/(K_{xy} + \langle x\rangle)]$ (C1), and $\langle y_x\rangle = (k_{xy}/\mu_y)[K_{xy}/(K_{xy}+\langle x\rangle)]$ (I1). The total output population ($\langle y\rangle$) in our additive signal integration scheme is given by $\langle y\rangle = \langle y_s\rangle + \langle y_x\rangle$. Next, we record the steady-state copy number (co)variances,

$$\Sigma^F_s = \langle s\rangle, \tag{2a}$$

$$\Sigma^F_{sx} = \frac{\langle f'_{x,s}\rangle \Sigma^F_s}{(\mu_s + \mu_x)}, \tag{2b}$$

$$\Sigma^F_{sy} = \frac{\langle f'_{y,s}\rangle \Sigma^F_s + \langle f'_{y,x}\rangle \Sigma^F_{sx}}{(\mu_s + \mu_y)}, \tag{2c}$$

$$\Sigma^F_x = \langle x\rangle + \frac{\langle f'_{x,s}\rangle \Sigma^F_{sx}}{\mu_x}, \tag{2d}$$

$$\Sigma^F_{xy} = \frac{\langle f'_{y,s}\rangle \Sigma^F_{sx} + \langle f'_{x,s}\rangle \Sigma^F_{sy} + \langle f'_{y,x}\rangle \Sigma^F_x}{(\mu_x + \mu_y)}, \tag{2e}$$

$$\Sigma^F_y = \langle y\rangle + \frac{\langle f'_{y,s}\rangle \Sigma^F_{sy} + \langle f'_{y,x}\rangle \Sigma^F_{xy}}{\mu_y}. \tag{2f}$$

The superscript F implies that these expressions belong to the generic FFL structure. The notation $\langle f'_{x,s}\rangle$ stands for $df_x(s)/ds$ evaluated at $s = \langle s\rangle$, and so on for other input functions. Now that we have modeled the FFL, it is easier to connect the gene products to the specifics of the PID principle. Figure 1(c) schematically depicts the relationships that the pairwise information [$I^F(y;s)$ and $I^F(y;x)$] and total information [$I^F(y;s,x)$] share with the unique, redundant, and synergistic information.

II. PATHWAY-DEPENDENT DECOMPOSITION FRAMEWORK FOR INFORMATION REDUNDANCY AND EXTRINSIC NOISE

The MMI PID principle prescribes $R^F(y;s,x) \equiv R^F_y \stackrel{\text{def}}{=} \min\{I^F(y;s), I^F(y;x)\}$ [19]. To implement a redundancy decomposition involving both of the parallel signal decoding pathways, we restrict to parametric setups that conform to the constraint $I^F(y;s) < I^F(y;x)$. This means that the information redundancy is numerically identical to the signal fidelity between input and output species, i.e., $R^F_y = I^F(y;s)$. To avoid any conceptual confusion, we should note that their physical interpretations are quite different from each other as described in Sec. I. This information is computed using $I^F(y;s) \stackrel{\text{def}}{=} \Sigma^F_y - \Sigma^F_{y|s}$ [19,34,35]. The last term is the partial variance of y when conditioned on s and follows from $\Sigma^F_{y|s} \stackrel{\text{def}}{=} \Sigma^F_y - (\Sigma^{F\,2}_{sy}/\Sigma^F_s)$ [19,36]. Thus, we arrive at $R^F_y = \Sigma^{F\,2}_{sy}/\Sigma^F_s$. Now, we turn our attention to Eq. (2c) and rewrite the steady-state covariance between the master regulator and output species as follows:

$$\Sigma^F_{sy} = \begin{cases} \underbrace{\langle y_s\rangle(1-P_{sy})\Phi_{ys}}_{\Sigma^O_{sy}\text{ from } S\to Y} + \overbrace{\frac{\langle x_s\rangle\langle y_x\rangle}{\langle x\rangle}(1-P_{sx})(1-P_{xy})\Phi_{xs}\Phi_{ys}}^{\Sigma^T_{sy}\text{ from } S\to X\to Y} & \text{(C1)}, \\ \overbrace{\langle y_s\rangle(1-P_{sy})\Phi_{ys}}^{\Sigma^O_{sy}\text{ from } S\to Y} - \underbrace{\frac{\langle x_s\rangle\langle y_x\rangle}{\langle x\rangle}(1-P_{sx})P_{xy}\Phi_{xs}\Phi_{ys}}_{\Sigma^T_{sy}\text{ from } S\to X\dashv Y} & \text{(I1)}. \end{cases} \tag{3}$$

$\Phi_{ij} =: [\mu_i/(\mu_i + \mu_j)]$ capture the internode separation of timescales and are involved in downward filtration of regulatory fluctuations through temporal averaging [37]. P_{ij} denote steady-state promoter occupancy probabilities, e.g., $P_{sx} = [\langle s\rangle/(K_{sx} + \langle s\rangle)] = [\sigma^b_{sx}\langle s\rangle/(\sigma^u_{sx} + \sigma^b_{sx}\langle s\rangle)]$. Other $P_{\ldots}$ follow similar expressions. Equation (3) makes it evident that this covariance is a mixture of two components. The contribution from the one-step cascade ($S \to Y$) is common to both FFLs. The remaining portion originates from the two-step cascade ($S \to X \to Y$ or $S \to X \dashv Y$). Their respective magnitudes are denoted by Σ^O_{sy} and Σ^T_{sy}. This covariance decomposition, i.e., $\Sigma^F_{sy} = \Sigma^O_{sy} \pm \Sigma^T_{sy}$, signifies that fluctuations flowing along the parallel pathways interfere at the output node constructively and destructively for the C1- and I1-FFLs, respectively.

Using the last expression, we can reexpress R^F_y in terms of its pathway-centric terms as follows:

$$R^F_y = \frac{{\Sigma^F_{sy}}^2}{\Sigma^F_s} \tag{4a}$$

$$= \underbrace{\frac{{\Sigma^O_{sy}}^2}{\Sigma^F_s}}_{\| \; R^O_y} + \underbrace{\frac{{\Sigma^T_{sy}}^2}{\Sigma^F_s}}_{\| \; R^T_y} \pm \underbrace{2\frac{\Sigma^O_{sy}\Sigma^T_{sy}}{\Sigma^F_s}}_{\| \; R^C_y}. \tag{4b}$$

In Eq. (4b), the + and − signatures in front of R^C_y stand for the C1- and I1-FFLs, respectively. R^O_y and R^T_y are the redundant information stemming from the one-step and two-step cascades, respectively. R^C_y is the cross redundancy produced by interpathway interference in the fluctuations. $R^F_y = R^O_y + R^T_y \pm R^C_y$ unequivocally suggests the impact of regulatory interactions on the superposition of submodular common information sharing elements. Now, we consider measuring the noise extrinsically transmitted from the master regulator to the final gene product. Looking at the expression of the output variance in Eq. (2f), we can distinguish $\langle y\rangle$ as a measure of its intrinsic variability. On the other side, the covariances, i.e., Σ^F_{sy} and Σ^F_{xy}, represent extrinsic factors of fluctuations [38,39]. A comparison between Eqs. 2(c) and 2(e) suggests that the metric of Σ^F_{sy} is functionally independent of Σ^F_{xy}. Hence, we prefer the former covariance to compute the population-normalized extrinsic noise [25,39] as

$$N^F_{sy} \overset{\text{def}}{=} \frac{\left|\Sigma^F_{sy}\right|}{\langle s\rangle\langle y\rangle} \tag{5a}$$

$$= \left| \langle y_s\rangle^f \underbrace{\frac{\Sigma^O_{sy}}{\langle s\rangle\langle y_s\rangle}}_{\| \; N^O_{sy}} \pm \langle y_x\rangle^f \underbrace{\frac{\Sigma^T_{sy}}{\langle s\rangle\langle y_x\rangle}}_{\| \; N^T_{sy}} \right| \left(\because \Sigma^F_{sy} = \Sigma^O_{sy} \pm \Sigma^T_{sy}\right). \tag{5b}$$

Here, $\langle y_i\rangle^f =: \langle y_i\rangle/\langle y\rangle$ measure the normalized output synthesis capacities of the individual cascades. Equation 5(b) implies that the one-step and two-step cascades, respectively, transfer N^O_{sy} and N^T_{sy} amounts of noise to the output node in the process of decoding the input signal. As in the redundancy case, the C1- and I1-FFLs follow different rules, i.e., $N^F_{sy} = |\langle y_s\rangle^f N^O_{sy} \pm \langle y_x\rangle^f N^T_{sy}|$, to assemble the pathway-specific noise flows. While the C1-FFL produces the composite extrinsic noise by summing up the weighted elementary noise flows, the I1-FFL takes into account the corresponding difference. By consulting Eqs. 4(b) and 5(b) and using $\Sigma^F_s = \langle s\rangle$ from Eq. (2a), we underline the following trade-offs between redundancy and extrinsic noise both at the submodular and full-motif levels:

$$R^O_y = \langle s\rangle\langle y_s\rangle^2 {N^O_{sy}}^2, \tag{6a}$$

$$R^T_y = \langle s\rangle\langle y_x\rangle^2 {N^T_{sy}}^2, \tag{6b}$$

$$R^C_y = 2\langle s\rangle\langle y_s\rangle\langle y_x\rangle N^O_{sy}N^T_{sy}, \tag{6c}$$

$$R^F_y = \langle s\rangle\langle y\rangle^2 {N^F_{sy}}^2. \tag{6d}$$

Equations 6(a)–6(d) convey that with increased (decreased) extrinsic noise flow from input to output node, the inter-regulator common information sharing invariably increases (decreases). In other words, redundant information processing and extrinsic noise transmission are intimately interconnected.

Equations 4(a) and 5(a), in association with Eq. (3), are used, respectively, to compute the analytical R^F_y and N^F_{sy}. The corresponding pathway-resolved elements are explicitly expressed in terms of biochemical parameters and species abundances as follows:

$$R^O_y = \frac{\langle y_s\rangle^2}{\langle s\rangle}(1 - P_{sy})^2\Phi^2_{ys} \text{ (C1 and I1)}, \tag{7}$$

$$R^T_y = \begin{cases} \frac{\langle x_s\rangle^2\langle y_x\rangle^2}{\langle s\rangle\langle x\rangle^2}(1 - P_{sx})^2(1 - P_{xy})^2\Phi^2_{xs}\Phi^2_{ys} & \text{(C1)} \\ \frac{\langle x_s\rangle^2\langle y_x\rangle^2}{\langle s\rangle\langle x\rangle^2}(1 - P_{sx})^2P^2_{xy}\Phi^2_{xs}\Phi^2_{ys} & \text{(I1)}, \end{cases} \tag{8}$$

$$R^C_y = \begin{cases} \frac{2\langle x_s\rangle\langle y_s\rangle\langle y_x\rangle}{\langle s\rangle\langle x\rangle}(1 - P_{sy})(1 - P_{sx})(1 - P_{xy})\Phi_{xs}\Phi^2_{ys} & \text{(C1)} \\ \frac{2\langle x_s\rangle\langle y_s\rangle\langle y_x\rangle}{\langle s\rangle\langle x\rangle}(1 - P_{sy})(1 - P_{sx})P_{xy}\Phi_{xs}\Phi^2_{ys} & \text{(I1)}, \end{cases} \tag{9}$$

$$N^O_{sy} = \frac{1}{\langle s\rangle}(1 - P_{sy})\Phi_{ys} \text{ (C1 and I1)}, \tag{10}$$

$$N^T_{sy} = \begin{cases} \frac{\langle x_s\rangle}{\langle s\rangle\langle x\rangle}(1 - P_{sx})(1 - P_{xy})\Phi_{xs}\Phi_{ys} & \text{(C1)} \\ \frac{\langle x_s\rangle}{\langle s\rangle\langle x\rangle}(1 - P_{sx})P_{xy}\Phi_{xs}\Phi_{ys} & \text{(I1)}. \end{cases} \tag{11}$$

To validate our LNA-based results, we implement the stochastic simulation algorithm (SSA) [40]. Here, we should mention that the usage of Hill functions to model gene regulation is an approximation in contrast with elementary mass-action kinetics [26,41]. The coarse-grained origin of the Hill functions assumes fast binding and unbinding events between regulatory proteins and their target promoters in comparison with other timescales in the network. In doing so, binding fluctuations are excluded in the regulator copy numbers. Recently, Holehouse and Grima demonstrated that for positive and negative feedback models, the usage of Hill functions is only justified when the protein-DNA binding rate is considerably smaller than the unbinding rate [28]. Besides, application of the heuristic SSA sometimes underestimates the noise level for Hill-type input functions [42]. Hence, such modeling approach is not suitable for all parametric regimes of a gene regulation network. Previously, Ref. [31] reported that the LNA can yield exact results up to second moments even for certain systems with second-order reactions. But, the

presence of deterministic bistability and stochastic bimodality causes the breakdown of LNA. These features are often exhibited by genetic systems with simpler architectures than the FFL. For example, in an autoregulatory switch, stochastic bimodality emerges for a large parameter range even when the deterministic description is monostable [43]. This is also the case for a genetic toggle switch without cooperativity but in the presence of multiplicative noise [44]. Hence, we choose our parameter sets that conform to monostable and monomodal FFL configurations. We should mention that the signals are always *on* in our model, i.e., none of the genes switch between their individual active and inactive states. Finally, as a cautionary remark, we note that the need for monomodal parameter regimes presents quite a limitation on the methodology utilized in this paper. In Sec. III, the LNA- and SSA-based datasets are, respectively, represented by solid lines and symbols. The latter are generated using steady-state ensemble averages of $O(10^5)$ independent time series for each of the separate constructs.

III. RESULTS AND DISCUSSION

A. Controlling information redundancy and extrinsic noise via the direct regulatory pathway's activation strength

In our first parametric setup, we maintain equal output productions by the parallel signal decoding cascades, i.e., $\langle y_s\rangle = \langle y_x\rangle = 50$ copies. $\langle x_s\rangle$ ($\langle x_{ur}\rangle$) increases (decreases) within 0–100 (100–0) to keep $\langle x\rangle$ fixed at 100. Additionally, $\langle s\rangle = 100$ is maintained throughout the network transformation. Changing K_{sy} implies that the master regulator-mediated maximal output production rate (k_{sy}) is altered following the constraint: $k_{sy} = \mu_y\langle y_s\rangle[1 + (K_{sy}/\langle s\rangle)]$. k_{xy} may be changed in a similar fashion. Fixed output abundance helps to compare different network configurations on an equitable footing, which may be interpreted as a robust fitness trait. This can be experimentally achieved by altering the RNA polymerase-promoter interaction strength [9]. Ultimately, these distinct genotypes ($\{k_{sy}, k_{xy}\}$) map onto a unique phenotype ($\langle y\rangle$). This is consistent with experimental observations on the *lac* system of *E. coli*, which shows remarkable optimization to achieve maximal expression levels [45]. Choosing a tunable direct activation coefficient comes from the following consideration. Compared to the two-step cascade, the one-step cascade can respond to the input signal quite easily, thereby quickly initiating the output production. Depending upon the reliability of the inducer signal, this may not be an accurate decision all the time. Thus, a tunable direct activation coefficient helps the regulatory machinery to mount gene expression only when the inducer signal is of significance. Following Ref. [46], we assign $K_{sx} = 10\langle s\rangle$, $K_{xy} = 10\langle x\rangle$ (C1), and $K_{xy} = \langle x\rangle$ (I1). To ensure $R_y^F = I^F(y;s)$, we make the following three choices for the one-step cascade: $K_{sy} = \{0.5,\ 0.1,\ 0.01\} \times \langle s\rangle$. Thus, we can probe a broad range of binding conditions between the master regulator and output promoter.

Our first choice, i.e., $K_{sy} = 0.5\langle s\rangle$, implies that 50 copies of S mount the half-maximal production of $\langle y_s\rangle$. Figures 2(a) and 2(b) show the resulting profiles of $\{R_y^F, N_{sy}^F\}$ for the two FFL types. Both metrics monotonically increase with growing $\langle x_s\rangle$ for the C1-FFL. In the I1-FFL, their response is

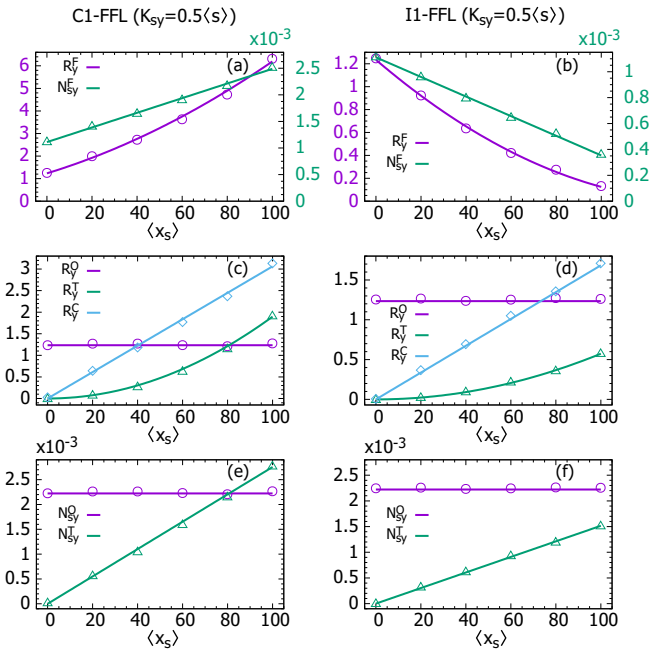

FIG. 2. (a), (b) The profiles of $\{R_y^F, N_{sy}^F\}$ for the C1- and I1-FFLs, respectively. $\langle s\rangle = \langle x\rangle = \langle y\rangle = 100$, $\langle y_s\rangle = \langle y_x\rangle = 50$ are maintained. Other parameters are $\mu_s = \mu_x = 0.5$, $\mu_y = 1.0$, all in min^{-1}, and $K_{sx} = 10\langle s\rangle$, $K_{sy} = 0.5\langle s\rangle$, $K_{xy} = 10\langle x\rangle$ (C1), and $K_{xy} = \langle x\rangle$ (I1). The associated $k_{...}$ are determined from the steady-state version of Eqs. (1a)–(1c). The pathway-resolved redundancy and extrinsic noise components are shown in (c)–(f). Their correlation dependencies follow from Eqs. (7)–(11). The redundancy-noise association agrees with Eqs. (6a)–(6d). The FFL-level differences in the redundancy and extrinsic noise trends vanish in the submodular level.

completely opposite. Their behavior attests to the fact that the information redundancy does depend on the interdriver correlation strength. To rationalize the profiles, we need to explore their pathway-resolved components from Eqs. (7)–(11) in Figs. 2(c)–2(f). They indeed suggest the existence of a correlation-independent redundancy element, namely, R_y^O. R_y^T and R_y^C grow parabolically and linearly with $\langle x_s\rangle$, respectively. On the noise front, N_{sy}^O is the correlation-independent component that corresponds to R_y^O. Similar to R_y^T, N_{sy}^T rises with the interdriver correlation. Due to a common type of one-step cascade, $\{R_y^O, N_{sy}^O\}$ are invariant across FFLs. However, $\{R_y^T, R_y^C, N_{sy}^T\}$ take different values due to the regulatory dissimilarity of the two-step cascades. A one-to-one association between composite and submodular $\{R_y^{\cdots}, N_{sy}^{\cdots}\}$ is confirmed through Eqs. (6a)–(6d). Although the composite metrics characteristically differ from each other in the FFL variants, the respective submodular elements are consistent in their responses to an increasing $\langle x_s\rangle$. It is only through the formulas: $R_y^F = R_y^O + R_y^T \pm R_y^C$ and $N_{sy}^F = |\langle y_s\rangle^f N_{sy}^O \pm \langle y_x\rangle^f N_{sy}^T|$ that we can appreciate how submodular redundancy and extrinsic noise elements manufacture differences in distinct FFLs. To elaborate on this issue, we point out the following. Figure 2(b) portrays diminishing N_{sy}^F when increasing $\langle x_s\rangle$ opens up

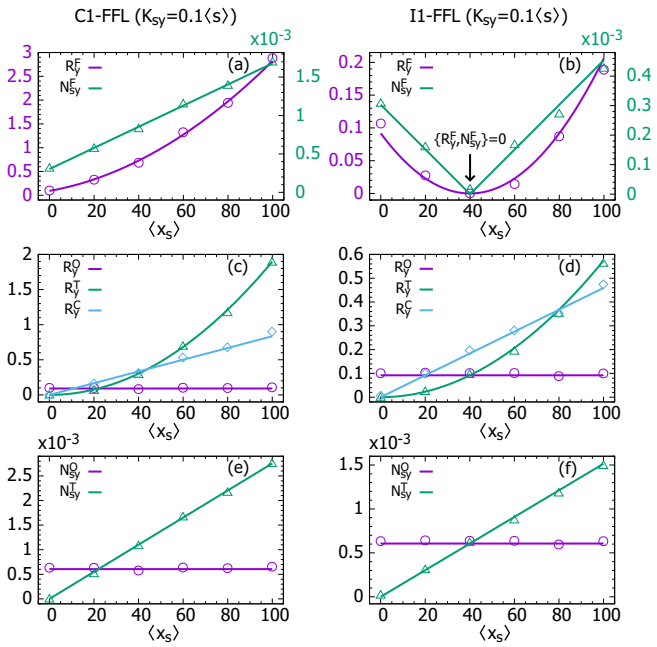

FIG. 3. Keeping other independent parameters the same as in our control Fig. 2, we make $K_{sy} = 0.1\langle s\rangle$. (a), (b) $\{R_y^F, N_{sy}^F\}$ for the C1- and I1-FFLs, respectively. In (b), an arrow marks the $\langle x_s\rangle$ value at which the composite redundancy and extrinsic noise are completely quenched. (c)–(f) The respective pathway-resolved metrics.

another channel ($S \to X$) for noise flow in addition to the existing $S \to Y$. Naturally, one expects increased transmission of upstream fluctuations to the output node in this situation. This is precisely what we find by looking at N_{sy}^T in Fig. 2(f). To accommodate this intuitively antithetical scenario, we are guided by the above-mentioned decomposition rule for the I1-FFL. Here, a constant N_{sy}^O and a negative signature accompanying N_{sy}^T engineer the decaying N_{sy}^F. This negative signature bears testimony to the regulatorily mismatched parallel cascades in the I1-FFL. The destructive interference in redundancy quantified by R_y^C gradually disentangles the pairwise information spaces, namely, $I^F(y;s)$ and $I^F(y;x)$, thereby reducing their overlap region [see Fig. 1(c)]. Hence, the commonly shared information between the regulators about the target (R_y^F) diminishes with increasing $\langle x_s\rangle$ in the composite I1-FFL.

Figure 3 illustrates $\{R_y^{\cdots}, N_{sy}^{\cdots}\}$ for $K_{sy} = 0.1\langle s\rangle$, i.e., when half of $\langle y_s\rangle$ is synthesized by 10 copies of S. With this increase in direct activation strength ($\propto K_{sy}^{-1}$), the binding of S with its output promoter gets five-times tighter than in the control setup of Fig. 2. In Fig. 3(a), the C1-FFL preserves the increasing trends of $\{R_y^F, N_{sy}^F\}$ from Fig. 2(a). Their reduced magnitudes result from significant drops in $\{R_y^O, N_{sy}^O\}$ as shown in Figs. 3(c) and 3(e). The changes in the one-step cascade-controlled elements accompany lowering of R_y^C at par with Eq. (9). An interesting situation arises for the I1-FFL in Fig. 3(b), where R_y^F displays a concave-up profile closely followed by N_{sy}^F. Both of them are completely extinguished at a unique value of $\langle x_s\rangle$. Equations (4b), (5b), and (7)–(11) determine the precise numerical value of this correlation strength,

$$\langle x_s\rangle|_{\{R_y^F, N_{sy}^F\}=0} = \frac{\langle y_s\rangle\langle x\rangle(1-P_{sy})}{\langle y_x\rangle(1-P_{sx})P_{xy}\Phi_{xs}}. \tag{12}$$

Here again, we can verify that the redundancy and extrinsic noise components displayed in Figs. 3(d) and 3(f) are superposed according to the respective Eqs. (4b) and (5b) to produce the effective metrics in Fig. 3(b). This shows that even sufficiently correlated predictor species may produce zero redundant information about their target when the composite I1-FFL is considered. Analysis at the full-motif level masks the nonzero redundancies generated by the constituent pathways. Besides, Fig. 3(b) firmly connects information redundancy to extrinsic noise flow from input to output node in FFLs. It is noteworthy that an analysis focusing only on the C1-FFL would have obscured the full picture concerning the interplay among redundancy, correlation, and extrinsic noise. It is R_y^C that nullifies $R_y^O + R_y^T$ and gives $R_y^F = 0$. Similarly, the balancing act between N_{sy}^O and N_{sy}^T finally quenches N_{sy}^F. It can be further shown from Eqs. (7)–(9) that at the particular value of $\langle x_s\rangle = 40$ given by Eq. (12), $R_y^O = R_y^T = R_y^C/2$ [see, also, Fig. 3(d)]. Therefore, a strong destructive interpathway crosstalk is implemented by R_y^C with this particular magnitude and thus $I^F(y;s)$ and $I^F(y;x)$ are completely decoupled. Hence, the redundant information vanishes in the composite I1-FFL.

Our final parametric setup considers $K_{sy} = 0.01\langle s\rangle$, implying only one copy of S is able to produce half of $\langle y_s\rangle$. This is the maximum binding strength achievable by the one-step cascade. The resulting redundancy and extrinsic noise datasets are profiled in Fig. 4. As expected from our previous deliberation, Fig. 4(a) shows that $\{R_y^F, N_{sy}^F\}$ are further diminished in their magnitudes for the C1-FFL. The I1-FFL continues to produce new trends as $\{R_y^F, N_{sy}^F\}$ now rise with increasing $\langle x_s\rangle$ in Fig. 4(b). With the present supertight binding in the one-step cascade, N_{sy}^O is so small that $\{R_y^O, R_y^C\}$ are also minimized. Naturally, N_{sy}^T and R_y^T are the dominant factors in this situation. Here, the destructive interference induced by R_y^C is not sufficient enough to dampen the common information sharing [the overlap between $I^F(y;s)$ and $I^F(y;x)$] in the composite I1-FFL. Hence, even in the presence of $X \dashv Y$, R_y^F grows with increasing $\langle x_s\rangle$. Under the current circumstances, the FFLs become information-theoretically similar to the corresponding two-step cascades. In this scenario, we observe $I^F(y;s,x) \approx I^F(y;x)$ (data not shown). This has a substantial bearing on the interaction information or net synergy [19]: $\Delta I = I^F(y;s,x) - I^F(y;s) - I^F(y;x) \approx -I^F(y;s) = -R_y^F$. In earlier works, we hypothesized that the underlying Markov chain structure of a two-step cascade generates net information redundancy [47,48]. The present parametrization transforms fully functional FFLs into information-theoretic two-step cascades poised at redundancy. This happens in spite of the one-step cascade synthesizing half of the total output population. Figures 2–4 suggest that the I1-FFL, due to its regulatory architecture, has an advantage over the C1-FFL in producing varied redundancy and extrinsic noise responses.

We close this section by providing a quantitative assessment of the changes in the pathway-specified redundancies and extrinsic noise as K_{sy} is tuned. If the direct activation

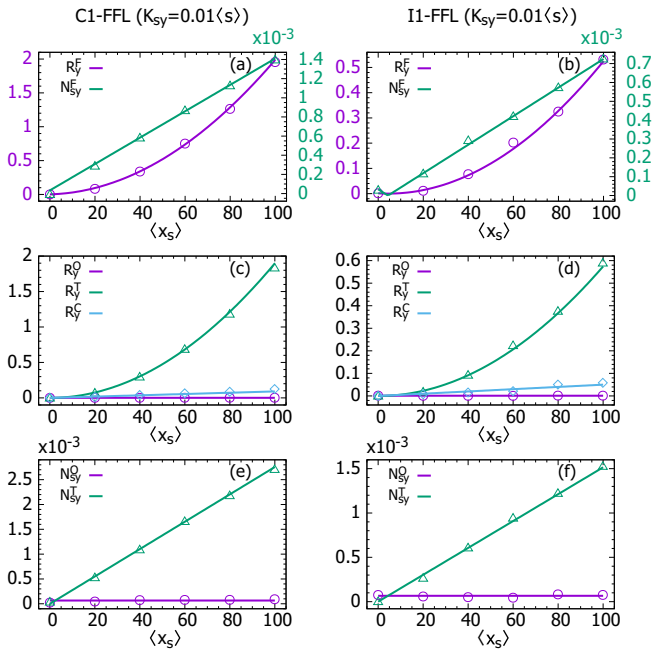

FIG. 4. We implement the strongest direct activation of the output gene by setting $K_{sy} = 0.01\langle s\rangle$. Other independent parametric considerations are identical with previous setups. (a) and (b) capture the composite redundancy and extrinsic noise, both of which show similar trends in the C1- and I1-FFLs. The submodular metrics in (c)–(f) document minimal R_y^O and N_{sy}^O.

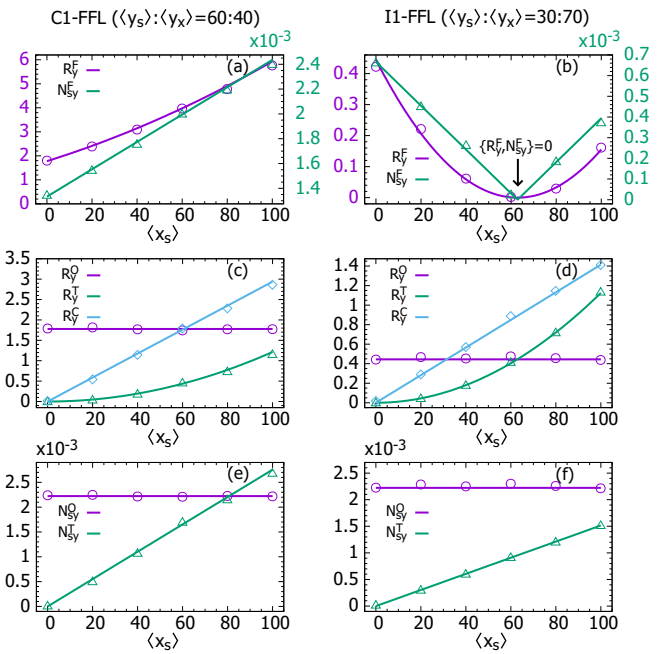

FIG. 5. Results showing the redundancy and extrinsic noise responses for unequal output production capacities of the direct and indirect pathways. $\langle y_s\rangle : \langle y_x\rangle = 60:40,\ 30:70$ are maintained for the C1- and I1-FFLs, respectively. Other independent parametric conditions remain the same as in the control Fig. 2. $\{R_y^F, N_{sy}^F\}$ in (b) show similar trends as in Fig. 3(b). The monotonic metric features in (a) are the same as in previous instances of the C1-FFL. (c) and (d) suggest simultaneous control over $\{R_y^O, R_y^T, R_y^C\}$ with respect to the corresponding control Figs. 2(c) and 2(d). Comparison between Figs. 2(e) and 2(f) and Figs. 5(e) and 5(f) reveals that N_{sy}^O and N_{sy}^T are invariant to the $p_{\langle y_s\rangle}$ transformation.

coefficient (ac) is made $1/p_{ac}$ times its former value, where $p_{ac} > 1$, the relevant metrics in the strong-binding (SB) and weak-binding (WB) conditions are inter-related through

$$R_y^O\big|_{\rm SB} = [1 + (p_{ac} - 1)P_{sy}|_{\rm WB}]^{-2} R_y^O\big|_{\rm WB}, \tag{13a}$$

$$R_y^C\big|_{\rm SB} = [1 + (p_{ac} - 1)P_{sy}|_{\rm WB}]^{-1} R_y^C\big|_{\rm WB}, \tag{13b}$$

$$N_{sy}^O\big|_{\rm SB} = [1 + (p_{ac} - 1)P_{sy}|_{\rm WB}]^{-1} N_{sy}^O\big|_{\rm WB}. \tag{13c}$$

B. Effects of unbalanced direct and indirect signal decodings on information redundancy and extrinsic noise

Equations (7)–(9) indicate the nonlinear dependence of pathway-resolved redundancies on $\{\langle y_s\rangle, \langle y_x\rangle\}$. The population-normalized extrinsic noise components are naturally invariant to the parallel pathways' output production capacities [see Eqs. (10) and (11)]. Datasets in Sec. III A considered balanced signal decodings, i.e., $\langle y_s\rangle = \langle y_x\rangle = 50$ copies. Here, we make them unbalanced while keeping $\langle y\rangle = 100$ copies as before. With $K_{sy} = 0.5\langle s\rangle$ as in Fig. 2, the maximal output production rates, namely, $\{k_{sy}, k_{xy}\}$, are modified accordingly. In general, if $\langle y_s\rangle$ is made $p_{\langle y_s\rangle}$ times its previous value ($\langle y_s\rangle \to p_{\langle y_s\rangle} \times \langle y_s\rangle$), Eqs. (7)–(9) obey the following transformation rules:

$$R_y^O \xrightarrow{p_{\langle y_s\rangle}} p_{\langle y_s\rangle}^2 R_y^O, \tag{14a}$$

$$R_y^T \xrightarrow{p_{\langle y_s\rangle}} \left[1 + (1 - p_{\langle y_s\rangle})\frac{\langle y_s\rangle}{\langle y_x\rangle}\right]^2 R_y^T, \tag{14b}$$

$$R_y^C \xrightarrow{p_{\langle y_s\rangle}} p_{\langle y_s\rangle}\left[1 + (1 - p_{\langle y_s\rangle})\frac{\langle y_s\rangle}{\langle y_x\rangle}\right] R_y^C. \tag{14c}$$

Although the submodular extrinsic noise components remain unchanged, their respective weightages ($\langle y_i\rangle^f$) in the superposition given by Eq. (5b) are now unequal. Hence, N_{sy}^F in Figs. 5(a) and 5(b) differ from the control Figs. 2(a) and 2(b), respectively. In Fig. 5(a), the C1-FFL preserves the monotonic nature of $\{R_y^F, N_{sy}^F\}$ from previous setups. The constituent redundancies change according to Eqs. (14a)–(14c) and are plotted in Fig. 5(c). The invariant extrinsic noise elements are shown in Fig. 5(e). Their weightages manage the pathway susceptibilities to the intrinsic noise (variability) of S. The latter is expressed as $N_s^F \overset{\rm def}{=} \Sigma_s^F/\langle s\rangle^2 = \langle s\rangle^{-1}$ [using Eq. (2a)]. Reexpressing Eq. (5b) makes this issue easier for the C1-FFL:

$$N_{sy}^F = \Bigg[\langle y_s\rangle^f (1 - P_{sy})\Phi_{ys} + \frac{\langle x_s\rangle\langle y_x\rangle^f}{\langle x\rangle}(1 - P_{sx})(1 - P_{xy})\Phi_{xs}\Phi_{ys}\Bigg] \times N_s^F. \tag{15}$$

Therefore, changed output productions from individual pathways alter the total extrinsic noise without modifying its basic components.

The trends similar to Fig. 3(b) reappear in Fig. 5(b) for the I1-FFL. Here, again, the I1-FFL manufactures $\{R_y^F, N_{sy}^F\} = 0$ in the presence of a strong inter-regulator activating edge.

The elemental redundancies are appropriately modified in Fig. 5(d). The current setup exemplifies complete attenuation of redundancy and extrinsic noise for the composite I1-FFL when the motif transforms its decoding branches from a balanced to an unbalanced state. Perturbing the individual extrinsic noise transduction is not a prerequisite in this case, as verified by Fig. 5(f). Here, the interpathway regulatory mismatch ensures that for certain $\langle x_s\rangle$ and $\langle y_i\rangle^f$, the proportions of N_s^F flowing through the decoding cascades balance each other. This may be analytically verified via

$$N_{sy}^F = \left| \langle y_s\rangle^f (1-P_{sy})\Phi_{ys} - \frac{\langle x_s\rangle\langle y_x\rangle^f}{\langle x\rangle}(1-P_{sx})P_{xy}\Phi_{xs}\Phi_{ys} \right| \times N_s^F. \tag{16}$$

Similar to Fig. 3(d), it can be directly checked from Eqs. (7)–(9) that for the unique $\langle x_s\rangle$ value suggested by Eq. (12), the I1-FFL produces $R_y^O = R_y^T = R_y^C/2$, as shown in Fig. 5(d). Consequently, R_y^C completely separates $I^F(y;s)$ and $I^F(y;x)$ engineering $R_y^F = 0$.

C. Growing co-regulator abundance exerts hyperbolic control over redundant information and extrinsic noise propagation

Until now, we have considered fixed $\langle x\rangle$ (100 copies) while $\langle x_s\rangle$ increases from 0 to 100 copies. This is attained by simultaneously decreasing $\langle x_{ur}\rangle$ from 100 to 0 copies following $\langle x_{ur}\rangle = \langle x\rangle - \langle x_s\rangle$. Here, we conceive of a situation in which $\langle x_{ur}\rangle = 10$ copies with $\langle x_s\rangle$ increasing like before. Hence, $\langle x\rangle$ increases from 10 to 110 copies. Other stand-alone parameters remain unchanged from their control values in Fig. 2. The network modification factors in the fixed and increasing $\langle x\rangle$ cases are $\langle x_s\rangle$ and $\langle x_s\rangle/(\langle x_{ur}\rangle + \langle x_s\rangle)$, respectively. The latter sigmoidal function introduces saturating effects to $\{R_y^F, N_{sy}^F\}$, profiled in Figs. 6(a) and 6(b). Contrasted with their counterparts in Figs. 2(a) and 2(b), they hyperbolically rise and fall for the C1- and I1-FFLs, respectively. Naturally, the one-step cascade-mediated components (R_y^O and N_{sy}^O) are indifferent to growing co-regulator abundance. The features of R_y^T, R_y^C, and N_{sy}^T in Figs. 6(c)–6(f) explain that of Figs. 6(a) and 6(b). To fully appreciate the implications of variable co-regulator population, we invoke its intrinsic noise: $N_x^F \overset{\text{def}}{=} \langle x\rangle^{-1} = (\langle x_{ur}\rangle + \langle x_s\rangle)^{-1}$. For fixed $\langle x_{ur}\rangle$, linearly increasing $\langle x_s\rangle$ inevitably forces N_x^F to drop hyperbolically. Its effect on the relevant metrics are gathered from Eqs. (8), (9), and (11):

$$R_y^T \propto \left[\langle x_s\rangle N_x^F\right]^2, \tag{17a}$$

$$R_y^C \propto \langle x_s\rangle N_x^F, \tag{17b}$$

$$N_{sy}^T \propto \langle x_s\rangle N_x^F. \tag{17c}$$

Figures 6(a) and 6(b) are better understood with these relations along with the superposition rules: $R_y^F = R_y^O + R_y^T \pm R_y^C$ and $N_{sy}^F = |\langle y_s\rangle^f N_{sy}^O \pm \langle y_x\rangle^f N_{sy}^T|$. The current analysis directs our attention to a couple of biochemical mechanisms through which the regulators may establish their commonly shared information content. As the inter-regulator edge is enhanced, the FFLs may require a robust (fixed) co-regulator population level. Other parameters remaining fixed, the motifs

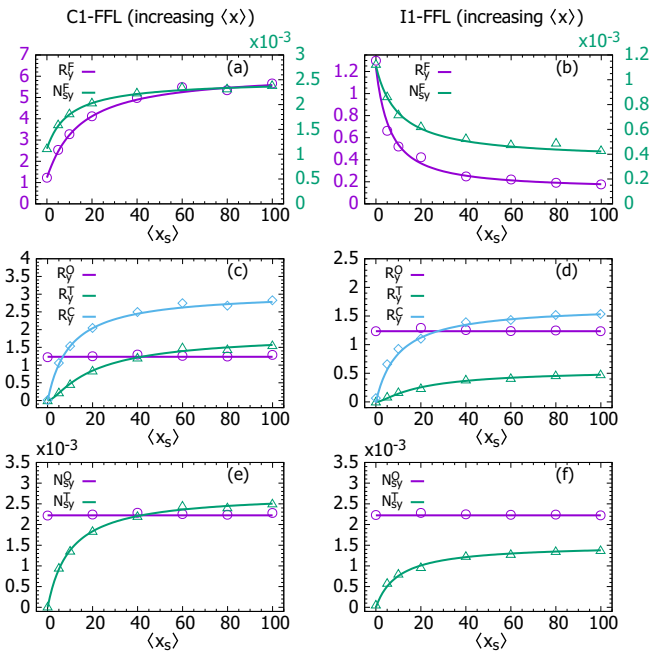

FIG. 6. With Fig. 2 as our control setup, $\langle x_{ur}\rangle = 10$ and $\langle x_s\rangle \in [0, 100]$ produce hyperbolic trends in $\{R_y^F, N_{sy}^F\}$ as shown in (a) and (b). Their constituent elements are depicted in (c)–(f).

then gain in R_y^T and R_y^C by raising $\langle x_s\rangle$ without tuning the co-regulator's intrinsic variability. In the absence of such phenotypic robustness, this variability is diminished to accelerate redundant information processing.

IV. CONCLUSION

The formalism of MMI PID implies that redundant information which is commonly shared between the driver variables is invariant to the interdriver correlation. To scrutinize this claim in sufficient detail, we employed the C1- and I1-FFLs with tunable inter-regulator edges and quantified information redundancy in a variety of biochemically realistic parametric configurations. Additionally, we assessed the extrinsic noise propagation from input to output node in these motifs. Using the variance-based concept of information in a Gaussian context, we deconstructed information redundancy produced by the composite FFL into three distinct components at the submodular level. Apart from the redundancies handled individually by the constituent one-step and two-step cascades, the interpathway signaling interference generates a cross-redundancy element. Similar analysis revealed the separate shares of the two decoding branches in the overall extrinsic noise. Unlike the redundancy, the noise propagation is free of any cross-pathway element. We conducted our study on three independent parametric realizations. These are dictated by (i) the tunable activation coefficient of the one-step cascade, (ii) asymmetrical output production capacities of the cascades, and (iii) the growing co-regulator population. The first two setups kept the total co-regulator expression level constant. Both of them showed that the one-step cascade-mediated information redundancy is indeed independent of interdriver correlation, whereas the component due to

the two-step cascade maintains a quadratic relationship. The cross redundancy linearly grows with the correlation. With increasing co-regulator population, the redundancy element from the two-step cascade shows hyperbolic tendency and so does the cross redundancy. However, the one-step cascade redundancy retains its correlation invariance. In all of these cases, the extrinsic noise elements from the parallel cascades exhibit correlation dependencies relatable to the associated redundancies. Our analytical estimates predict that each of the submodular and composite redundancies nonlinearly relies on the corresponding extrinsic noise components.

The composite metrics show monotonic growths for the C1-FFL. In sharp contrast, the I1-FFL produces a wide range of responses. This is due to an interpathway regulatory mismatch created by the inhibitory edge between the co-regulator and the output of the I1-FFL. As a result, the input fluctuations flowing via the parallel decoding branches interfere constructively and destructively at the output node for the C1- and I1-FFLs, respectively. Consequently, these two FFLs are distinct in combining their elementary redundancy and extrinsic noise contributions. The cross redundancy upgrades and downgrades the summed pathway redundancies for the C1- and I1-FFLs, respectively. For the extrinsic noise, a mere weighted sum and difference of the pathway-dependent noise flows distinguish these respective FFLs. Hence, with suitable activation coefficients and pathway-specific output production capacities, the I1-FFL unveils nonmonotonic redundancy and extrinsic noise. The quenching of information redundancy shared by sufficiently correlated regulators is a special feature of the I1-FFL. The growth (decay) in total extrinsic noise translates itself into an increasing (diminishing) total redundancy. Furthermore, the latter is extinguished in the absence of the former. The growing co-regulator abundance allows for an enhanced control over redundancy and extrinsic noise transduction. Their effective contributions quickly reach high (C1) or low (I1) values. Results compiled from this varied parametric repertoire showcase the subtle correlation dependencies of redundant information. They also provide good evidence in favor of a close connection between redundant information and extrinsic noise in FFLs. To boost inter-regulator redundant information sharing targeting the output, the master regulator also needs to enhance noise supply to the output. The C1- and I1-FFLs generally differ from each other in processing redundant information and transducing extrinsic noise in their composite structures. Thanks to the metric deconstruction formulas, we can clearly see that their submodular characteristics are similar in different FFLs. The cross redundancy precisely quantifies the over- and underestimation of common information sharing between the two hierarchical structural levels and thus provides a measure of emerging complexity.

Since FFLs are recurrent beyond gene regulation, e.g., in neuronal nets [9,11], our findings may generate some insights there. In recent years, the incoherent FFL has been studied in the context of adaptation [49–51]. The diverse redundancy response of the I1-FFL may emerge as a key player in the adaptive sensory systems. On the other hand, cascades of coherent FFLs are functional in the *B. subtilis* sporulation [52]. The role of multivariate information filtered via a sequence of FFLs in developmental decision making is still an open research problem. Previously, this covariance-based interpretation of extrinsic noise was used to rationalize the abundance statistics of the FFL class of motifs [46]. As shown in the present communication, this type of extrinsic noise is easily decomposable into pathway-specified components and can be directly connected to the variance-based information. Besides, this specific metric has been generalized for nonequivalent reporters to decompose noise in TNF–NF-κB–JNK and TNF–NF-κB–ATF-2 signaling nets [53]. An alternative framework conceives of the extrinsic (environmental) noise as fluctuating reaction rates [32,54]. Notably, Shahrezaei *et al.* showed that the coherent (incoherent) FFLs amplify (attenuate) noise [54]. Interestingly, our current analyses reveal a more nuanced performance of the I1-FFL in noise transmission. In Ref. [55], Lestas and colleagues proved an information-noise correspondence in a generic feedback circuit. Their study pinpointed the information source in biomolecular abundance fluctuations. Therefore, we can safely infer that the redundancy-extrinsic noise trade-off in FFLs is a fundamental aspect of biochemical signaling channels.

For the evolution of a multi-input-output net, multivariate information acts as a candidate fitness function that favors signal-integrating nets [56]. Multivariate information processing often indicates pathological states, e.g., the presence of synergy in epileptic brain and *HeLa* cell line [57]. For physical systems such as the two-dimensional Ising model, multivariate information transfer successfully anticipates the critical transition [58,59]. These findings highlight the urgent need to expand the widely used pairwise information-based frameworks for biochemical networks. Earlier studies hypothesized that cascades and branched motifs with net redundancy simultaneously benefit from increased signal-to-noise ratio [47,60]. Further refinements in the redundancy-noise trade-off may propel efficient motif design by synthetic means. At present, some evidence is available in *E. coli* to support gene expression noise as an evolvable trait [61–64]. It remains an open question whether life forms can also get naturally selected based on their information-processing capabilities. Moreover, we hope that the intricate interplay of information and correlation may usher in a better understanding of information decomposition protocols in dynamical systems.

ACKNOWLEDGMENT

The author acknowledges the research support from Bose Institute, Kolkata.

[1] S. F. Taylor, N. Tishby, and W. Bialek, arXiv:0712.4382.

[2] W. Bialek, *Biophysics: Searching for Principles* (Princeton University Press, Princeton, 2012).

[3] A. Erez, T. A. Byrd, M. Vennettilli, and A. Mugler, Phys. Rev. Lett. **125**, 048103 (2020).

[4] P. Mehta, S. Goyal, T. Long, B. L. Bassler, and N. S. Wingreen, Mol. Syst. Biol. **5**, 325 (2009).

[5] R. Cheong, A. Rhee, C. J. Wang, I. Nemenman, and A. Levchenko, Science **334**, 354 (2011).
[6] M. D. Petkova, G. Tkačik, W. Bialek, E. F. Wieschaus, and T. Gregor, Cell **176**, 844 (2019).
[7] C. G. Bowsher and P. S. Swain, Curr. Opin. Biotechnol. **28**, 149 (2014).
[8] A. Borst and F. E. Theunissen, Nat. Neurosci. **2**, 947 (1999).
[9] U. Alon, *An Introduction to Systems Biology: Design Principles of Biological Circuits*, 2nd ed. (CRC Press, Boca Raton, FL, 2020).
[10] B. Soufi, K. Krug, A. Harst, and B. Macek, Front. Microbiol. **6**, 103 (2015).
[11] R. Milo, S. Shen-Orr, S. Itzkovitz, N. Kashtan, D. Chklovskii, and U. Alon, Science **298**, 824 (2002).
[12] U. Alon, Nat. Rev. Genet. **8**, 450 (2007).
[13] S. Mangan and U. Alon, Proc. Natl. Acad. Sci. USA **100**, 11980 (2003).
[14] S. Mangan, A. Zaslaver, and U. Alon, J. Mol. Biol. **334**, 197 (2003).
[15] S. Mangan, S. Itzkovitz, A. Zaslaver, and U. Alon, J. Mol. Biol. **356**, 1073 (2006).
[16] S. Kalir, S. Mangan, and U. Alon, Mol. Syst. Biol. **1**, 2005.0006 (2005).
[17] C. E. Shannon, Bell. Syst. Tech. J. **27**, 379 (1948).
[18] P. L. Williams and R. D. Beer, arXiv:1004.2515.
[19] A. B. Barrett, Phys. Rev. E **91**, 052802 (2015).
[20] M. Harder, C. Salge, and D. Polani, Phys. Rev. E **87**, 012130 (2013).
[21] V. Griffith and C. Koch, in *Guided Self-organization: Inception, Emergence, Complexity and Computation* (Springer, Berlin, 2014), Vol. 9, pp. 159–190.
[22] N. Bertschinger, J. Rauh, E. Olbrich, J. Jost, and N. Ay, Entropy **16**, 2161 (2014).
[23] A. Eldar and M. B. Elowitz, Nature (London) **467**, 167 (2010).
[24] L. S. Tsimring, Rep. Prog. Phys. **77**, 026601 (2014).
[25] M. B. Elowitz, A. J. Levine, E. D. Siggia, and P. S. Swain, Science **297**, 1183 (2002).
[26] N. G. van Kampen, *Stochastic Processes in Physics and Chemistry*, 3rd ed. (North-Holland, Amsterdam, 2007).
[27] D. T. Gillespie, J. Chem. Phys. **113**, 297 (2000).
[28] J. Holehouse and R. Grima, Biophys. J. **117**, 1311 (2019).
[29] J. Elf and M. Ehrenberg, Genome Res. **13**, 2475 (2003).
[30] A. M. Walczak, G. Tkačik, and W. Bialek, Phys. Rev. E **81**, 041905 (2010).
[31] R. Grima, Phys. Rev. E **92**, 042124 (2015).
[32] E. M. Keizer, B. Bastian, R. W. Smith, R. Grima, and C. Fleck, Phys. Rev. E **99**, 052417 (2019).
[33] E. Ziv, I. Nemenman, and C. H. Wiggins, PLoS ONE **2**, e1077 (2007).
[34] L. Angelini, M. de Tommaso, D. Marinazzo, L. Nitti, M. Pellicoro, and S. Stramaglia, Phys. Rev. E **81**, 037201 (2010).
[35] S. Stramaglia, L. Angelini, G. Wu, J. M. Cortes, L. Faes, and D. Marinazzo, IEEE Trans. Biomed. Eng. **63**, 2518 (2016).
[36] L. Barnett, A. B. Barrett, and A. K. Seth, Phys. Rev. Lett. **103**, 238701 (2009).
[37] G. Tkačik, T. Gregor, and W. Bialek, PLoS ONE **3**, e2774 (2008).
[38] J. Paulsson, Nature (London) **427**, 415 (2004).
[39] J. Paulsson, Phys. Life Rev. **2**, 157 (2005).
[40] D. T. Gillespie, Annu. Rev. Phys. Chem. **58**, 35 (2007).
[41] D. Schnoerr, G. Sanguinetti, and R. Grima, J. Phys. A: Math. Theor. **50**, 093001 (2017).
[42] P. Thomas, A. V. Straube, and R. Grima, BMC Syst. Biol. **6**, 39 (2012).
[43] J. Holehouse, Z. Cao, and R. Grima, Biophys. J. **118**, 1517 (2020).
[44] T. Biancalani and M. Assaf, Phys. Rev. Lett. **115**, 208101 (2015).
[45] E. Dekel and U. Alon, Nature (London) **436**, 588 (2005).
[46] Md Sorique Aziz Momin and A. Biswas, Phys. Rev. E **101**, 052411 (2020).
[47] A. Biswas and S. K. Banik, Phys. Rev. E **93**, 052422 (2016).
[48] A. Biswas, Chaos **29**, 063108 (2019).
[49] W. Ma, A. Trusina, H. El-Samad, W. A. Lim, and C. Tang, Cell **138**, 760 (2009).
[50] G. T. Reeves, J. Biol. Eng. **13**, 62 (2019).
[51] P. Bhattacharya, K. Raman, and A. K. Tangirala, doi:10.1101/2021.05.27.445914.
[52] J. Narula, S. N. Devi, M. Fujita, and O. A. Igoshin, Proc. Natl. Acad. Sci. USA **109**, E3513 (2012).
[53] A. Rhee, R. Cheong, and A. Levchenko, Proc. Natl. Acad. Sci. USA **111**, 17330 (2014).
[54] V. Shahrezaei, J. F. Ollivier, and P. S. Swain, Mol. Syst. Biol. **4**, 196 (2008).
[55] I. Lestas, G. Vinnicombe, and J. Paulsson, Nature (London) **467**, 174 (2010).
[56] A. Tareen, N. S. Wingreen, and R. Mukhopadhyay, Phys. Rev. E (RC) **97**, 020402 (2018).
[57] S. Stramaglia, J. M. Cortes, and D. Marinazzo, New J. Phys. **16**, 105003 (2014).
[58] L. Barnett, J. T. Lizier, M. Harré, A. K. Seth, and T. Bossomaier, Phys. Rev. Lett. **111**, 177203 (2013).
[59] D. Marinazzo, L. Angelini, M. Pellicoro, and S. Stramaglia, Phys. Rev. E (RC) **99**, 040101 (2019).
[60] A. Biswas and S. K. Banik, Chaos **28**, 103102 (2018).
[61] K. Sato, Y. Ito, T. Yomo, and K. Kaneko, Proc. Natl. Acad. Sci. USA **100**, 14086 (2003).
[62] K. Kaneko and C. Furusawa, J. Theor. Biol. **240**, 78 (2006).
[63] L. Wolf, O. K. Silander, and E. van Nimwegen, eLife **4**, e05856 (2015).
[64] A. Urchueguía, L. Galbusera, D. Chauvin, G. Bellement, T. Julou, and E. van Nimwegen, PLoS Biol. **19**, e3001491 (2021).